6.6 ON THE ROLE OF DROP SIZE DISTRIBUTION IN TRMM RAIN PROFILING ALGORITHM

A. Tokay*[1,2], R. Meneghini[2], J. Kwiatkowski[2,3], E. Amitai[1,2], T. Kozu[5], T. Iguchi[4], C. Williams[6], M. Kulie[2,3], and C. Wilson[7]

[1] JCET/UMBC, Baltimore, MD
[2] NASA/GSFC, Greenbelt MD
[3] CEOSR/GMU, Fairfax, VA
[4] CRL, Koganei, Tokyo, Japan
[5] SU, Matsue, Japan
[6] CIRES/U. Colorado, Boulder, CO
[7] CLRC/RAL, Oxfordshire, UK

1. INRODUCTION

The selection of the drop size distribution (DSD) model is one of the critical steps in rain profiling algorithm (RPA) of the NASA Tropical Rainfall Measuring Mission (TRMM) (Iguchi et al. 2000). RPA requires R-Z_e and K-Z_e relations for convective and stratiform precipitation, where K and Z_e represent the attenuation and equivalent reflectivity at 13.8 GHz, respectively, and R is the rain rate. These relations are derived from several samples of DSD measurements. An averaging is performed among the K-Z_e and R-Z_e relations to determine the *initial* coefficients and exponents for the profiling algorithm. The *final* coefficients and exponents are determined through surface reference technique (Meneghini et al. 2000). The convective stratiform partitioning is determined based on the DSD characteristics (Kozu et al. 2001). RPA, however, determines the precipitation type from three-dimensional characteristics of reflectivity following Awaka et al. (1985) and Steiner et al. (1995, SHY95 hereafter). The goal of this study is to investigate the variations in the DSD and its impact on K-Z_e and R-Z_e relations due to differences in climatic regimes and due to the differences in precipitation type algorithms.

2. DROP SIZE DISTRIBUTION MEASUREMENTS

The DSD measurements were collected by Joss-Waldgovel disdrometers at eight different sites (Table 1). At most of the sites, the disdrometer was located within a dense rain gauge network and a radar coverage. At some sites, vertically pointing radar (profiler) was also available. After the quality control, one minute averaged DSD observations are classified either convective or stratiform based on a relationship between mass weighted drop diameter (D_m) and R. Similarly, Tokay and Short (1996) used a relation between intercept parameter of gamma function (N_0) and R. Unlike N_0, D_m is directly calculated from observed DSD without fitting a mathematical function. Here, all the spectra having R≥25 mmh^{-1} is assigned convective. The discrimination between the two types of precipitation is decided following $D_{mass}=1.02\ R^{0.25}$, where D_{mass} is the mass weighted drop diameter calculated from rain rate. If $D_m>D_{mass}$, the spectrum has more large drops at a given rain rate and is classified stratiform, otherwise convective. This algorithm is applied to all the sites. The disdrometer algorithm is rather simple and requires refinement, but this is the beyond to scope of this study.

Most of the DSD samples were collected during 2 to 4 months long field campaigns (Table 1). Therefore, our knowledge on the precipitation type is based on rather limited sample. For instance, DARWIN-94 disdrometer measurements were mostly taken during monsoon period resulting in higher percentage of stratiform occurrence. In Kwajalein (KWAJEX), rain total was dominated by convective precipitation, while stratiform rain had a relatively high percentage of rainfall in western tropical Pacific Ocean (COARE). In all sites, most of rainfall fell in convective form, while stratiform rain was observed most of the time. A drastic example of this changeover was observed in South China Sea Monsoon Experiment (SCSMEX), where abrupt very intense but short convective showers dominated the rain totals. The convective fraction of rain volume and occurrence were about the same in Southwest Amazon basin of Brazil (TRMM-LBA) and in Central Florida (TEFLUN-B). The DSD measurements in Gadanki, India, and Singapore were collected for a longer period of time, permitting to study monthly and seasonal variations of DSD and rainfall.

Table 1. Occurrence and volume of convective rain in the tropics. The experiment period and rain duration are also shown.

Experiment	Dates	Duration (minutes)	Convective (occur./vol.)
COARE	11/5/92-2/11/93	8770	31%, 70%
DARWIN-94	1/15/94-3/6/94	5660	26%, 76%
SCSMEX	4/5/98-6/8/98	4204	30%, 82%
TEFLUN-B	7/29/98-9/25/98	2941	33%, 78%
TRMM-LBA	1/17/99-3/2/99	4750	34%, 78%
KWAJEX	7/14/99-8/29/99	4251	37%, 84%
GADANKI-99	5/3/99-12/22/99	8782	33%, 68%
SINGAPORE	4/27/00-9/30/00	7034	21%, 74%

Table 2. The rain totals measured directly by disdrometer, and calculated from reflectivity utilizing site specific and version 5 of the TRMM RPA dual R-Z_e relations. The percentage bias between measured and calculated rain totals are also shown.

Experiment	Rain Total (mea.; mm)	Rain Total (site; mm)	Rain Total (RPA; mm)
COARE	573	572 (<1%)	569 (-6%)
DARWIN-94	373	385 (3%)	380 (2%)
SCSMEX	423	425 (<1%)	467 (11%)
TEFLUN-B	274	284 (3%)	420 (53%)
TRMM-LBA	292	321 (10%)	401 (37%)
KWAJEX	376	400 (6%)	387 (3%)
GADANKI-99	446	474 (6%)	592 (33%)
SINGAPORE	505	530 (5%)	713 (41%)

Table 1 of Iguchi et al. (2000) presents the following relations $R = 0.04024\ Z_e^{0.6434}$ and $R = 0.02282\ Z_e^{0.6727}$ for convective and stratiform rain, respectively. Utilizing these and site specific dual R-Z_e relations, rain totals are calculated from disdrometer reflectivities and compared with the rain total that is calculated directly from DSD measurements (Table 2). Except COARE, site specific and RPA R-Z_e relations overestimate the rainfall. The former R-Z_e overestimates the true rainfall up to 10%. This is partially due to the regression method. Here, the linear least-squares fit on a log-log scale is

**Corresponding author address*: Ali Tokay, NASA Goddard Space Flight Center, Code 912.1, Greenbelt, MD 20771; e-mail: tokay@radar.gsfc.nasa.gov

employed. The nonlinear least squares fit reduce the absolute bias between the measured and estimated rain totals (Campos and Zawadzki 2000). The RPA R-Z_e pair represents well oceanic, but not continental rainfall. Perhaps, precipitation may be reclassified not only as convective and stratiform but also as continental and oceanic rain. In this case, special attention should be given to the regions that exhibit seasonal reversal of winds and therefore dual precipitation modes.

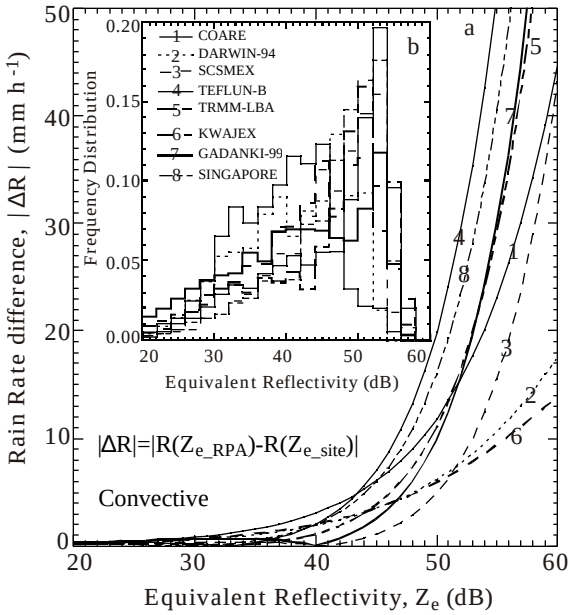

Fig. 1. Absolute difference in rain rate, |ΔR|, (a) and the frequency distributions of rain volume (b) as a function of reflectivity in convective rain. |

Figure 1a presents absolute difference rain rate, |ΔR|, as a function of Z_e in convective rain. The |ΔR| is due to the difference between site specific and RPA R-Z_e relations. This analysis helps to evaluate the applicability of the RPA R-Z_e relation to a specific region, but it is limited with disdrometer observations period. The difference in R increases with Z_e such that it is at least 5 mmh^{-1} at 50 dBZ_e for all the sites. Although dramatic increases in |ΔR| are evident at most of the sites at above 40-50 dBZ_e, it is important to determine the Z_e range where most of the rain falls. Fig. 1b shows the histograms of the convective rain as a function of Z_e. The histograms for Central Florida and Singapore are skewed to the higher reflectivities peaking at 52-54 dBZ_e. A sharp increase in |ΔR| is observed above 40 dBZ_e for these two sites. This reflects the dramatic differences in rain totals in the last two columns of Table 2. In Darwin and Kwajalein, the |ΔR| increases more gradually with Z_e and the rainfall is mostly contributed at 38-52 dBZ_e range. The difference in rain totals in Table 2 is rather minimal for these two sites. In western tropical Pacific Ocean, most of the rain (85%) is received between 30 and 50 dBZ_e range and |ΔR| for this range is less than 7 mmh^{-1}. This indicates that convective rain has less contribution from large drops than the other sites such as Central Florida and Singapore. In terms of R-Z_e relations, the coefficient is higher in western tropical Pacific Ocean than in Singapore and Central Florida assuming that R-Z_e curves do not cross each other. The presence of more large drops in Singapore and Central Florida may be indicative of frequent occurrence of short-lived intense convection. The combined observations of scanning and vertically pointing radars can provide an insight to the characteristic differences of precipitation in oceanic and continental regimes.

3. RAIN TYPE CLASSIFICATION ALGORITHMS

Three different precipitation classification algorithms are employed in this study. The algorithms are developed based on disdrometer, C-band Doppler radar, and dual frequency (915 MHz and 2835 MHz) profiler observations that were taken during a field campaign in Amazon basin of Brazil. The disdrometer and profiler were collocated and 54.4 km from radar. The radar scanned about every 10 minutes, while profilers sampled the atmosphere up to 10.5 km at 105 m pulse length every minute. The dwell time was 30 sec for both profilers. Here, 915 MHz profiler reflectivities at 105 m pulse height were primarily employed to determine the rain type. In a few rain events where the 915 MHz profiler observations had a wide data gap, 2835 MHz profiler observations are substituted.

Precipitation is classified either convective or stratiform. The disdrometer algorithm is as defined above and the radar algorithm examines the texture of the reflectivity field in 2x2 km^2 grid space similar to SHY95. The profiler algorithm seeks bright band (BB), a signature for stratiform rain. First, peak reflectivity ($Z_{e\ (peak)}$) is determined within 4 to 5 km. The top and bottom of the bright band was then found by examining the maximum curvature in the reflectivity profile (Fabry and Zawadzki 1995). Then, $Z_{e\ (rain)}$ and $Z_{e\ (snow)}$ were defined as adjacent gates just below the bottom and above the top of the bright band, respectively. A minimum reflectivity difference of 5 dB is required between $Z_{e\ (peak)}$ and $Z_{e\ (rain)}$ to satisfy the well-defined BB condition (Bellon et al. 1995). If the reflectivity difference is between 1 to 5 dB, the weak BB is present. For both well-defined and weak BB conditions, the difference between $Z_{e\ (peak)}$ and $Z_{e\ (snow)}$ is required to be 1 dB since the reflectivity profile is often slanted due to the wind shear where the cloud top is only in a few gates above the bright band. The BB is visually inspected for each rain event to evaluate the performance of the algorithm. Typically, the reflectivity profile below the BB does not change with height. However, an enhancement of reflectivity is noticed in a number of cases where the reflectivity profile is severely slanted. If the reflectivity below the bright band exceeds 40 dBZ, the profile is classified as convective. In the absence of bright band, profiler is classified as convective. Next, the echo top height is examined to distinguish shallow versus deep convective rain. If the echo tops are less than 4.5 km, the rain event is considered to be shallow convective. The shallow convective rain could either exist for the entire rain event or is observed at the early phase of deep convection. At some rain events, shallow but not convective rain is present at the tail of a long rain event following bright band. This segment of a rain event is classified as stratiform regardless of the absence of bright band.

A 70% and 84% agreement is found between the disdrometer and profiler algorithms in occurrence and rain volume, respectively (Table 3a). The disdrometer algorithm had 10%

more stratiform profiler than the profiler algorithm. This is partially due to the fact that BB is sufficient but not necessary criterion for stratiform rain and partially due to mis-classification by disdrometer.

Table 3. Rainfall statistics regarding (a) disdrometer vs. profiler, (b) disdrometer vs. radar, and (c) radar vs. profiler rain classification algorithms. The 2nd and 3rd columns show the number of cases in each category and its percentage contribution to the total occurrence, while 4th and 5th columns are the rain volume (mm) in each category and its percentage contribution to the total rain.

a

Precip Class	Str. (profiler)	Con. (profiler)	Str. (profiler)	Con. (profiler)
Str (disd)	1970 (47%)	827 (20%)	31(12%)	28 (11%)
Con (disd)	410 (10%)	373 (23%)	12 (5%)	180 (72%)

b

Precip Class	Str. (radar)	Con. (radar)	Str. (radar)	Con. (radar)
Str (disd)	166 (63%)	19 (7%)	3 (18%)	2 (15%)
Con (disd)	49 (18%)	31 (12%)	2 (11%)	8 (55%)

c

Precip Class	Str. (profiler)	Con. (profiler)	Str. (profiler)	Con. (profiler)
Con (rad)	147 (62%)	52 (22%)	2 (17%)	2 (11%)
Str (radar)	3 (1%)	35 (15%)	<1(4%)	10 (68%)

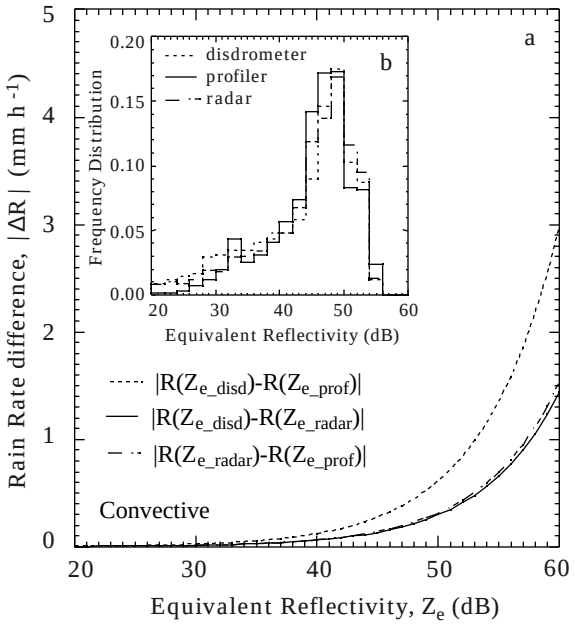

Fig. 2. Absolute difference in rain rate (a) and the frequency distributions of rain volume (b) as a function of reflectivity in convective rain.

A 63% and 73% agreement is found between the disdrometer and radar algorithms in occurrence and rain volume, respectively (Table 3b). The disdrometer algorithm had 11% less stratiform grids than the radar algorithm. Unlike profiler algorithm, radar algorithm first identifies the convective grids and the reminder nonzero reflectivity areas are classified as stratiform. Biggerstaff and Listemaa (2000) further studied the SHY95 rain algorithm by incorporating vertical structure of radar reflectivity. For unorganized and embedded convection, they converted more stratiform areas and rainfall to the convective areas and rainfall, while vice versa is true for squall lines. The misclassifications by the disdrometer algorithm also contribute the differences.

A 77% and 85% agreement is found between the radar and profiler algorithms in occurrence and volume, respectively (Table 3c). The profiler algorithm had 21% less stratiform profiles than the radar algorithm. The disagreement between profiler and radar algorithms was mainly in the form of no bright band with weak horizontal reflectivity gradient. This has been classified transition regime by Amitai (2000). Since the sampling interval of scanning radar is much longer than profiler and disdrometer, the sample of DSD measurements classified by radar is quite small. The disdrometer observations between the two successive radar scans are interpolated for the precipitation classification by radar. This allows to have a sufficient sample to derive the relations between the integral rain parameters.

Like Fig. 1a, Fig. 2a presents $|\Delta R|$ as a function of Z_e in convective rain, but the $|\Delta R|$ is due to the differences between radar, profiler, and disdrometer precipitation classification algorithms reflected on R-Z_e relations. Although $|\Delta R|$ due to the profiler and disdrometer classified R-Z_e is relatively higher than the other two pairs listed in Fig. 2., $|\Delta R|$ is less than 2 mmh^{-1} for the range of Z_e at which rain observed at the surface (Fig. 2b). This is an indicative that the disdrometer observations that are classified by three different algorithms do not result in substantial differences R-Z_e relations. These results are preliminary, however, major conclusions are not expected to change with refinement of the rain classification algorithms.

Acknowledgements, This study is supported by NASA TRMM program under Dr. R. Kakar. We would like to thank Drs. T. Keenan of BMRC, Australia, S. Yuter of University of Washington, and J. T. Ong, of Nanyang Technological. University, Singapore for providing disdrometer data.

REFERENCES

Amitai, E., 2000: Systematic variation of observed radar reflectivity-rainfall rate relations in the tropics. *J. Appl. Meteor.*, **39**, 2198-2208.

Awaka, J., Y. Furuhama, M. Hoshiyama, and A. Nishitsuji, 1985: Model calculations of scattering properties of spherical bright-band particles made of composite dielectrics. *J. Radi. Res. Lab.*, **32,** 73-87.

Bellon, A., I. Zawadzki, and F. Fabry, 1997: Measurements of melting layer attenuation at X-band frequencies. *Radio Science*, **32**, 943-955.

Biggerstaff, M. I., and S. A. Listemaa, 2000: An improved scheme for convective/stratiform echo classification using radar reflectivity. *J. Appl. Meteor.*, **39**, 2129-2150.

Campos, E., and I. Zawadzki, 2000: Instrument uncertainties in Z-R relations. *J. Appl. Meteor.*, **39**, 1088-1102.

Fabry F., and I. Zawadzki, 1995: The melting layer of precipitation: Radar observations and their interpretation. *J. Atmos. Sci.*, **52**, 838-851.

Iguchi, T., T. Kozu, R. Meneghini, J. Awaka, and K. Okamoto, 2000; Rain-profiling algorithm for the TRMM precipitation radar. *J. Appl. Meteor.*, **39**, 2038-2052.

Meneghini, R., T. Iguchi, T. Kozu, L. Liao, K. Okamoto, J. Jones, and J. Kwiatkowski, 2000: Use of the surface reference technique for path estimates from the TRMM precipitation radar. *J. Appl. Meteor.*, **39**, 22053-2070.

Steiner, M., R. A. Houze, and S. E. Yuter, 1995: Climatological characterization of three-dimensional storm structure from operational radar and rain gauge data. *J. Appl. Meteor.*, **34**, 1978-2007.

Tokay, A., and D. A. Short, 1996: Evidence from tropical raindrop spectra of the origin of rain from stratiform and convective clouds. *J. Appl. Meteor.*, **35**, 355-371.